

AD \_\_\_\_\_

GRANT NUMBER DAMD17-96-1-6265

TITLE: Structure and Inhibition of the neu/erbB-2 Receptor

PRINCIPAL INVESTIGATOR: Steven Smith

CONTRACTING ORGANIZATION: Yale University  
New Haven, CT 06520-8047

REPORT DATE: September 1997

TYPE OF REPORT: Annual

PREPARED FOR: Commander  
U.S. Army Medical Research and Materiel Command  
Fort Detrick, Frederick, Maryland 21702-5012

DISTRIBUTION STATEMENT: Approved for public release;  
distribution unlimited

The views, opinions and/or findings contained in this report are those of the author(s) and should not be construed as an official Department of the Army position, policy or decision unless so designated by other documentation.

DTIC QUALITY INSPECTED 3

19980113 090

# REPORT DOCUMENTATION PAGE

Form Approved

OMB No. 0704-0188

Public reporting burden for this collection of information is estimated to average 1 hour per response, including the time for reviewing instructions, searching existing data sources, gathering and maintaining the data needed, and completing and reviewing the collection of information. Send comments regarding this burden estimate or any other aspect of this collection of information, including suggestions for reducing this burden, to Washington Headquarters Services, Directorate for Information Operations and Reports, 1215 Jefferson Davis Highway, Suite 1204, Arlington, VA 22202-4302, and to the Office of Management and Budget, Paperwork Reduction Project (0704-0188), Washington, DC 20503.

1. AGENCY USE ONLY (Leave blank)		2. REPORT DATE September 1997	3. REPORT TYPE AND DATES COVERED Annual (1 Sep 96 - 31 Aug 97)	
4. TITLE AND SUBTITLE Structure and Inhibition of the neu/erbB-2 Receptor			5. FUNDING NUMBERS DAMD17-96-1-6265	
6. AUTHOR(S) Steven Smith				
7. PERFORMING ORGANIZATION NAME(S) AND ADDRESS(ES) Yale University New Haven, CT 06520-8047			8. PERFORMING ORGANIZATION REPORT NUMBER	
9. SPONSORING/MONITORING AGENCY NAME(S) AND ADDRESS(ES) Commander U.S. Army Medical Research and Materiel Command Fort Detrick, Frederick, Maryland 21702-5012			10. SPONSORING/MONITORING AGENCY REPORT NUMBER	
11. SUPPLEMENTARY NOTES				
12a. DISTRIBUTION / AVAILABILITY STATEMENT Approved for public release; distribution unlimited			12b. DISTRIBUTION CODE	
13. ABSTRACT (Maximum 200)  Uncontrolled cell transformation often results when the receptors on the cell surface are "turned on" even in the absence of a signaling hormone. Here, we have studied the structure of one critical membrane receptor, the neu/erbB-2 receptor, whose activation is often associated with breast cancer. The goal has been to obtain the three dimensional structure of the receptor's transmembrane domain and to establish the mechanism by which the V664E mutation leads to receptor activation. During the first year, novel NMR methods have provided accurate distance constraints within and between transmembrane helices, while polarized infrared measurements have established one additional helix-helix contact in the transmembrane dimer at position 661. Computational searches have generated low energy structures of the transmembrane dimer for both wild-type neu and activated neu*. A key structural feature of both structures is the packing of Gly 665 in the dimer interface. In neu*, hydrogen bonding interactions of the Glu 664 side chains to polar threonine hydroxyl groups stabilize the transmembrane dimer. These studies set the stage for the design of specific inhibitors which should target the polar threonine and glutamic acid residues as well as Gly 665 and Ala 661, both of which have small side chains and allow good packing interactions.				
14. SUBJECT TERMS Breast Cancer			15. NUMBER OF PAGES 36	
			16. PRICE CODE	
17. SECURITY CLASSIFICATION OF REPORT Unclassified	18. SECURITY CLASSIFICATION OF THIS PAGE Unclassified	19. SECURITY CLASSIFICATION OF ABSTRACT Unclassified	20. LIMITATION OF ABSTRACT Unlimited	

## FOREWORD

Opinions, interpretations, conclusions and recommendations are those of the author and are not necessarily endorsed by the U.S. Army.

\_\_\_\_ Where copyrighted material is quoted, permission has been obtained to use such material.

\_\_\_\_ Where material from documents designated for limited distribution is quoted, permission has been obtained to use the material.

\_\_\_\_ Citations of commercial organizations and trade names in this report do not constitute an official Department of Army endorsement or approval of the products or services of these organizations.

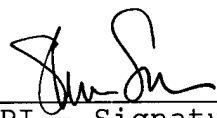
\_\_\_\_ In conducting research using animals, the investigator(s) adhered to the "Guide for the Care and Use of Laboratory Animals," prepared by the Committee on Care and Use of Laboratory Animals of the Institute of Laboratory Resources, National Research Council (NIH Publication No. 86-23, Revised 1985).

✓ \_\_\_\_ For the protection of human subjects, the investigator(s) adhered to policies of applicable Federal Law 45 CFR 46.

\_\_\_\_ In conducting research utilizing recombinant DNA technology, the investigator(s) adhered to current guidelines promulgated by the National Institutes of Health.

\_\_\_\_ In the conduct of research utilizing recombinant DNA, the investigator(s) adhered to the NIH Guidelines for Research Involving Recombinant DNA Molecules.

\_\_\_\_ In the conduct of research involving hazardous organisms, the investigator(s) adhered to the CDC-NIH Guide for Biosafety in Microbiological and Biomedical Laboratories.

  
\_\_\_\_  
PI - Signature

September 26, 1997  
\_\_\_\_  
Date

## TABLE OF CONTENTS

### Structure and Inhibition of the neu/erbB-2 Receptor

Front Cover	1
Report Documentation Page	2
Foreword	3
Introduction	5
Body	8
Conclusions	18
References	19
Appendices	22

## INTRODUCTION

Cancer results from a breakdown in the normal mechanisms which control the growth and division of cells. For many cells, the signals for initiating cell division are hormone molecules that bind to receptors on the surface of the cell. The signal is transmitted through the cell membrane by one or more receptor molecules. Receptors in an "active" state (with hormones bound) initiate a cascade of events which starts the replication machinery. Uncontrolled cell transformation often results when the receptors on the cell surface are "turned on" even in the absence of the signaling hormone. The research undertaken here has been to study the structure of one critical membrane receptor, the neu or erbB-2 receptor, whose activation has been associated with a large number of breast and ovarian cancers.

The neu receptor normally signals by dimerizing in response to hormone binding. The *neu/erbB-2* gene encodes a 185 kD receptor tyrosine kinase and is part of the erbB family of receptor tyrosine kinases; it has two cysteine-rich extracellular domains, a single helical membrane-spanning domain and an intracellular tyrosine kinase (TK) domain. Constitutive activation of the receptor is known to occur by gene overexpression or by a single mutation within the hydrophobic transmembrane sequence where a naturally-occurring valine residue at position 664 is replaced by glutamic acid [1-4]. The point mutation was the first occurrence of an activating mutation in the transmembrane domain of a growth factor receptor and has suggested that the structure of the transmembrane domain plays a larger role in the signal transduction process than previously thought. The goal of the research project has been to obtain the **three dimensional structure** of the neu receptor transmembrane domain and to establish the **mechanism** by which the Glu 664 mutation leads to receptor activation.

Figure 1 presents helical wheel diagrams of the neu (Val 664) and activated neu or "neu\*" (Glu 664) transmembrane domain. The sequences are largely hydrophobic. Of importance are the polar serine and threonine residues on the N-terminal side of position 664 and the glycine residue at position 665. Two models have been proposed for how the Val 664 → Glu 664 substitution causes cell transformation. The first involves a change in the secondary structure of the transmembrane (TM) domain. Brandt-Rauf et al. (1990) [5] calculated that the minimum-energy conformation in the region of Val 664 contains a sharp bend at positions 664 and 665, while the transforming sequence exists as an  $\alpha$ -helix. The second model is that the glutamate side chain promotes dimerization via hydrogen-bonding interactions [6]. In this case, the helices are thought to be held in the "active" state by hydrogen bonding between the Glu 664 carboxylic acid side chain on one helix and the Glu 664 side chain or peptide backbone carbonyl and amide groups of the second helix. Consistent with this model, the activated neu\* receptor has a higher propensity to form dimers than the normal neu (Val 664) receptor [7]. The position of the glutamic acid residue is sequence specific. Bargmann and Weinberg originally demonstrated that substitution of glutamic acid at positions 663 or 665 did not activate the receptor [1].

Stern and coworkers have undertaken an extensive mutagenesis study of the TM domain of neu to define the residues that are responsible for receptor activation [4]. They found that a sub-domain, -V<sub>663</sub>-E<sub>664</sub>-G<sub>665</sub>-, is important. The domain differs slightly from that predicted by Sternberg and Gullick [6], most notably in the importance of Ala 661 for receptor dimerization. Gullick and coworkers [8] have shown that intracellular expression of small proteins, corresponding to the TM and membrane-proximal domains of neu and containing variations on the activated neu TM

sequence, inhibits growth of neu transformed cells. However, a simple model involving hydrogen-bonding interactions of the Glu 664 may not be sufficient to explain receptor activation. Stern and coworkers [4] have shown, by moving the VEG sub-domain around in the TM sequence and by generating mutants that dimerize without activating the receptor, that dimerization alone is insufficient to cause cell transformation and that the interactions are likely to be highly specific. No direct evidence has been obtained for the points of contact in the receptor dimers and a high-resolution structure is needed to determine the exact nature of the protein interactions and whether they are distributed along the length of the TM domain.

In order to determine the structure of the transmembrane domain of the neu/erbB-2 receptor and address the molecular mechanism of receptor activation by the transforming Val 664 to Glu 664 mutation, magic angle spinning (MAS) NMR and polarized Fourier transform infrared (FTIR) studies have been undertaken. We have previously shown that MAS NMR and FTIR measurements provide a feasible approach for structural studies on membrane proteins [9-11].

MAS yields high resolution NMR spectra of membrane proteins in bilayer environments [6] and several different strategies have been developed for measuring weak dipolar couplings in MAS experiments [12-15]. Of importance for structural studies is that accurate internuclear distances can be derived from measurements of dipolar couplings which in turn provide constraints for generating and evaluating structural models. The two best established approaches are rotational resonance (RR) and rotational echo double resonance (REDOR) NMR. The RR NMR approach selectively restores the dipolar couplings by spinning the sample such that an integral multiple of the MAS frequency is equal to the chemical shift difference ( $\Delta\omega$ ) between two NMR resonances [16-18]. The distance limit for  $^{13}\text{C}\dots^{13}\text{C}$  measurements using RR NMR is  $\sim 6.5$  Å with resolution on the order of 0.3 Å. The REDOR NMR approach has been developed to measure weak heteronuclear dipolar couplings, such as those between  $^{31}\text{P}$  and  $^{13}\text{C}$  or  $^{15}\text{N}$  and  $^{13}\text{C}$  [19,20]. REDOR relies on the dephasing of magnetization of the observed spin through coupling to a second spin. The distance limit for  $^{13}\text{C}\dots^{15}\text{N}$  measurements using REDOR NMR is  $\sim 5$  Å with resolution on the order of 0.2 Å.

The global secondary structure and orientation of membrane proteins and peptides can be probed by polarized FTIR spectroscopy using the amide I vibration as a structurally sensitive marker [21]. The frequency of the amide I mode depends on hydrogen-bonding of the C=O group as well as on the geometry of the peptide backbone. Bands centered at  $\sim 1654$   $\text{cm}^{-1}$  correspond to  $\alpha$ -helical structures, while bands centered at  $1624 - 1637$   $\text{cm}^{-1}$  and  $1675$   $\text{cm}^{-1}$  correspond to the out-of-phase and in-phase modes of  $\beta$ -sheet structures, respectively or alternatively  $\beta$ -turn. Fourier self deconvolution (FSD) of the amide I region [22] can yield quantitative estimates of the relative ratios between the different secondary structural elements of the protein [23]. The orientation of the C=O group, which dominates the amide I vibration, can be derived from the relative absorption of IR light polarized parallel or perpendicular to the C=O transition dipole moment. Maximum absorption occurs when the polarization of light is parallel to the transition moment. In an  $\alpha$ -helix, the C=O transition dipole is known to be oriented at an angle of  $\sim 39^\circ$  relative to the helix axis [24-26].

During the first year of this research project, considerable progress has been made in establishing the high resolution structure of the neu receptor transmembrane domain. We have shown that the transmembrane domain forms a well-folded dimer of long helices oriented perpendicular to the membrane surface. MAS NMR methods for measuring internuclear distances have provided accurate distance constraints within and between transmembrane helices, while polarized infrared

measurements have established one additional helix-helix contact in the transmembrane dimer at position 661. In addition, computational searches have generated low energy structures of the transmembrane dimer in both *neu* and *neu\**. A key structural feature of both structures is the packing of the Gly 665 residues in the dimer interface. In the *neu\** TM dimer, hydrogen bonding interactions of the Glu 664 side chains to polar threonine hydroxyl groups across the helix interface stabilize the transmembrane dimer. The helices are predicted to cross in a right-handed coiled coil geometry.

During the next year of this project, additional NMR and IR measurements will be made to refine the current structure. In the original grant proposal, we planned to make measurements of association energies of *neu* transmembrane peptides with several different amino acid substitutions at position 664 as the first step in the design of competitive inhibitors. Based on the structural results and association energies, we had planned to design and synthesize organic inhibitors (peptide and non-peptide). Funding for this aspect of the project was withheld until a clinical collaboration was formed. This collaboration is now in place (see letter of collaboration from Prof. David Stern in the Department of Pathology at Yale University) and with the emerging structure of the *neu\** transmembrane dimer, we are encouraged that this phase of the research will be successful.

## BODY

### Experimental Methods

*Synthesis of neuTM and neu\*TM.* Peptides corresponding to the transmembrane domains of the neu (neuTM) and activated neu\* (neu\*TM) receptors were synthesized using solid-phase methods at the Keck Peptide Synthesis Facility at Yale University. The sequence of the 38-residue peptides corresponds to residues 649-686 in the neu receptor protein. The sequence of neu\*TM is shown below.

AEQRASPVTFILATV-E664-GVLLFLALVVVVGILIKRRRYK

The lyophilized peptide was dissolved in trifluoroacetic acid and purified using a 5 ml POROS-R1 reverse phase high performance liquid chromatography (RP-HPLC) column (Perceptive Biosystems, Cambridge, MA) equilibrated with 95% H<sub>2</sub>O, 2% acetonitrile and 3% 2-propanol. Peptide elution was achieved with a linear gradient to a final solvent composition of 5% H<sub>2</sub>O, 38% acetonitrile and 57% 2-propanol. All solvents contained 0.1% trifluoroacetic acid. Fractions containing peptides were then lyophilized and assessed for purity by amino acid analysis (correlation coefficients of > 0.95) and mass spectrometry. Following lyophilization, peptides were reconstituted into membranes as described in *Procedures* below.

*Fourier Transform Infrared Spectroscopy.* FTIR spectra were recorded on a Nicolet Magna 550 spectrometer purged with N<sub>2</sub> (Madison, WI) and equipped with a MCT/A detector. For transmission spectra, typically 50  $\mu$ l of sample (protein concentration of 36 - 90 mM) is dried on AgCl windows with dry air. For polarized ATR-FTIR spectra, the spectrometer was equipped with a KRS-5 wire grid polarizer (0.25 mm spacing, Grasbey Specac, Kent, UK). The sample (~300  $\mu$ l, 36 - 90 mM) was dried on the surface of a Ge internal reflection element and placed in a variable angle ATR accessory (Grasbey Specac, Kent, UK). Fourier self deconvolution (FSD) spectra were obtained using a bandwidth of 13 cm<sup>-1</sup> and an enhancement factor of 2.4, determined by Byler and Susi [23] to best fit experimental data. The helical content and orientation was determined using the approach described in our recent work on phospholamban [9].

For the SH exchange measurements, samples (300  $\mu$ l) containing 4 mg of dipalmitoyl-phosphatidylcholine (DPPC) and 0.4 mg of protein in a buffer of 0.1 mM Na<sub>2</sub>PO<sub>4</sub> pH 6.8 were centrifuged for 1 h in an A-95 rotor at 178,000g using an airfuge ultracentrifuge (Beckman, Palo Alto, CA). Pellets were resuspended in 75  $\mu$ l of either H<sub>2</sub>O or D<sub>2</sub>O and dried down on germanium IR windows following the procedure of Arkin et al. [31].

*Magic Angle Spinning NMR Spectroscopy.* MAS NMR experiments were performed on a Chemagnetics CMX 360 MHz spectrometer using a 5 mm high speed double resonance probe from Doty Scientific (Columbia, SC). The sample spinning speed for the rotational resonance experiments was kept constant to within 5 Hz using a spinning speed controller from Doty Scientific. The temperature was maintained at ca. +5°C or -50°C in order to slow residual rotational diffusion of the peptide which might otherwise average the dipolar couplings being measured. The pulse sequence used for the RR NMR experiments has been described previously [18]. Briefly, the sequence begins with <sup>1</sup>H-<sup>13</sup>C cross polarization to generate <sup>13</sup>C polarization that is then stored on the Z axis with a



$^{13}\text{C}$  flip-back pulse. One of the two  $^{13}\text{C}$  resonances is selectively inverted with a low power 500  $\mu\text{sec}$  pulse and magnetization is allowed to exchange between the two sites for a variable mixing period ( $t_m$ ). The power level of the inversion pulse is carefully adjusted to yield the maximum inversion. The distribution of  $^{13}\text{C}$  signal at the end of the mix period is detected with a  $90^\circ$  pulse that flips the magnetization into the transverse plane for acquisition of the NMR signal. Strong  $^1\text{H}$  decoupling is essential during the variable mix and acquisition periods. The decoupling power was set to a field strength of 83 kHz during the variable delay and acquisition. This level of decoupling was sufficient to maximize RR exchange as determined by a comparison of exchange rates at different decoupling field strengths. Conventional single amplitude CP was replaced by variable amplitude cross polarization (VACP) for these experiments to enhance the carbon signals at high MAS frequencies and yield more reliable intensities [32]. During the 5 msec CP contact time, the  $^{13}\text{C}$  amplitude corresponded to a constant spin-lock frequency of  $\sim 70$  kHz, while the proton amplitude was varied in nine steps each 555 msec in length. The first proton amplitude was centered at a  $B_1$  field strength of 70 kHz and the additional amplitudes were increased or decreased in  $\sim 2$  kHz steps. The VACP sequence yields stable and reproducible signals that are essential for generating the difference spectra and the magnetization exchange curves used for determining internuclear distances.

*Molecular Dynamics Simulations and Energy Minimization.* A computational search strategy using molecular dynamics and energy minimization procedures were employed to generate structural models of neuTM and neu\*TM [32]. Hydrogen atoms were introduced using the CHARMM22 parameter set with electrostatic and van der Waals energy terms enabled using the program X-PLOR in order to insure energetically reasonable initial positions for the hydrogen atoms.

## Assumptions

There are two assumptions that are implicit in the design of the proposed research project.

*Assumption 1. Peptides corresponding to the transmembrane sequence (plus  $\sim 10$  residues on each side) mimic the structure of the transmembrane sequence in the intact receptor.* The basis for this assumption is that the hydrophobic environment of the lipid bilayer controls the folding of the transmembrane sequence. As a result, the transmembrane sequence can be considered a protein domain whose structure is independent of the soluble domains of the protein, whose folding is controlled by an aqueous environment. Our FTIR and NMR measurements indicate that the peptides fold into regular secondary structure and exhibit quaternary contacts.

*Assumption 2. The mechanism of dimerization of the transmembrane peptides is the same as that in the intact receptor.* Support for this assumption must come from a comparison of the structural results on the transmembrane peptides with the biochemical/molecular biological results on the full length receptor. The structure we propose is consistent with the current literature on the full length receptor and provides the basis for the design of additional biochemical experiments.

## Procedures

*Reconstitution of neuTM and neu\*TM.* Reconstitution of the peptide fractions into membranes is a critical step in the structural studies undertaken in this research project. Simply put, if the

reconstituted peptide does not adopt a well-folded structure, then structural measurements are misleading at best. As a result, considerable time was placed into refining our reconstitution protocol. Two general reconstitution methods were tried and evaluated using polarized FTIR. The first method simply involved cosolubilization of purified lyophilized peptide and lipid in organic solvent, usually trifluoroethanol (TFE). Two different lipids were investigated: dipalmitoyl-phosphatidylcholine (DPPC) with a phase transition temperature of 42°C and dimyristoyl-phosphatidylcholine (DMPC) with a phase transition temperature of 24°C. The lipid-peptide solution was directly layered on the IR plate and the organic solvent was evaporated. Two variations of this method involved rehydration of the lipid-peptide film, followed by brief sonication before layering on the IR plate, and rehydration, sonication and incubation above the lipid phase transition. Simple evaporation and reconstitution gave dichroic ratios in an attenuated total reflection (ATR) experiment of <2.4, indicating that the peptide is not oriented. Rehydration and incubation generally increased the dichroic ratio to 2.8-3.0.

The second reconstitution method involved detergent dialysis. In this case, lipid, peptide (lyophilized) and detergent (octyl- $\beta$ -glucoside) were dissolved in trifluoroethanol (TFE). The TFE solution was lyophilized and the dry lipid/peptide/detergent mixture was rehydrated with phosphate buffer (10 mM phosphate and 50 mM NaCl, pH 7), such that the final concentration of octyl- $\beta$ -glucoside was 5%. The rehydrated sample was stirred slowly for at least 6 h and then the octyl- $\beta$ -glucoside was dialyzed using Spectra-Por dialysis tubing (3000 MW cutoff) for 24 hours against phosphate buffer at a temperature above the lipid phase transition. The reconstituted membranes were sonicated briefly (30-60 sec) in a ultrasonic bath and layered on a germanium crystal for IR measurements. An extension of the second method involved purification of the reconstituted membranes a 10-40% sucrose gradient. Centrifugation was carried out using a Beckman ultracentrifuge at 35,000 rpm (SW 41 rotor) for 8-12 h at 20°C. Generally, the reconstituted membranes form two discrete bands in the sucrose gradient. The upper band has a more homogeneous appearance and a higher lipid:peptide ratio as assessed by FTIR analysis. The lower band has an aggregated appearance and has a lower lipid:peptide ratio. The sucrose in each band was dialyzed against phosphate buffer for 24 hours. The best orientations (dichroic ratios of >3.2) were obtained from the upper band in the sucrose gradients. The orientation could usually be improved slightly by incubation. Moreover, the upper band in the sucrose gradients were largely free of non helical peptides that exhibited a 1630 cm<sup>-1</sup> amide I band.

Based on the results of these two approaches, the final protocol that was used for the structural studies leading to our current model was 1) detergent dialysis, 2) followed by sucrose gradients, 3) followed by incubation for 12h. After this last incubation step, 300  $\mu$ l of each sample were allocated for FTIR measurements, while the remainder was pelleted for MAS NMR experiments.

*Fourier Transform Infrared Spectroscopy.* The experimental design of the SH exchange experiment has been described previously [31]. Samples (300  $\mu$ l) containing 4 mg of DPPC and 0.4 mg of protein in a buffer of 0.1 mM Na<sub>2</sub>PO<sub>4</sub> pH 6.8 were centrifuged for 1 h in an A-95 rotor at 178,000g using an airfuge ultracentrifuge (Beckman, Palo Alto, CA). Pellets were resuspended in 75  $\mu$ l of either H<sub>2</sub>O or D<sub>2</sub>O and dried down on germanium IR windows following the procedure of Arkin et al. [31].

*Magic Angle Spinning NMR Spectroscopy.* The experimental design of the rotational resonance experiment has been described previously [18]. Briefly, the sequence begins with <sup>1</sup>H-<sup>13</sup>C cross

polarization to generate  $^{13}\text{C}$  polarization that is then stored on the Z axis with a  $^{13}\text{C}$  flip-back pulse. One of the two  $^{13}\text{C}$  resonances is selectively inverted with a low power 500  $\mu\text{sec}$  pulse and magnetization is allowed to exchange between the two sites for a variable mixing period ( $t_m$ ). The power level of the inversion pulse is carefully adjusted to yield the maximum inversion. The distribution of  $^{13}\text{C}$  signal at the end of the mix period is detected with a  $90^\circ$  pulse that flips the magnetization into the transverse plane for acquisition of the NMR signal. Strong  $^1\text{H}$  decoupling is essential during the variable mix and acquisition periods. The decoupling power was set to a field strength of 83 kHz during the variable delay and acquisition. This level of decoupling was sufficient to maximize RR exchange as determined by a comparison of exchange rates at different decoupling field strengths. Conventional single amplitude CP was replaced by variable amplitude cross polarization (VACP) for these experiments to enhance the carbon signals at high MAS frequencies and yield more reliable intensities [32]. During the 5 msec CP contact time, the  $^{13}\text{C}$  amplitude corresponded to a constant spin-lock frequency of  $\sim 70$  kHz, while the proton amplitude was varied in nine steps each 555 msec in length. The first proton amplitude was centered at a  $B_1$  field strength of 70 kHz and the additional amplitudes were increased or decreased in  $\sim 2$  kHz steps. The VACP sequence yields stable and reproducible signals that are essential for generating the difference spectra and the magnetization exchange curves used for determining internuclear distances.

*Molecular Dynamics Simulations and Energy Minimization.* The computational search strategy has been described previously by Adams et al. [32]. Low energy conformations of helix dimers were searched by rotating each helix through rotation angles  $\phi_1$  and  $\phi_2$  from  $0 - 360^\circ$  with a sampling size of  $45^\circ$ . The starting geometries included both left-handed and right-handed crossing angles. Four different runs were carried out for each starting geometry using simulated annealing of all atomic coordinates. The rotation and crossing angles were allowed to vary. The results of the search can be shown on a grid of  $\phi_1$  and  $\phi_2$ . The initial grid shows points separated by  $45^\circ$ . The final minimized structures, however, migrate from their initial geometries and often "cluster" in low energy wells. The individual structures in each low energy cluster are averaged.

## Results and Discussion

The technical objectives of the proposed research from the original proposal are outlined below. The first objective was to establish the high resolution structure of the neu (Val 664) and neu\* (Glu 664) transmembrane dimers in order to characterize the structural changes that are responsible for receptor activation. The results from Tasks 1-3 aimed at this objective are described below. The second objective was to synthesize competitive inhibitors to neu\* based on the structural results. The underlying premise of the proposed research is that high resolution structural data is essential for the design of inhibitors to the activated neu/erbB-2 receptor. Funding for the second objective was withheld until a clinical collaboration capable of testing synthesized inhibitors was established. This has been done and we are currently requesting funding for years 3-4.

### A. Structure of the neu and neu\* transmembrane and juxtamembrane sequences.

A.1 Magic angle spinning NMR spectroscopy. Internuclear distance measurements will be made using rotational resonance (RR) and rotational echo double resonance (REDOR) NMR methods to generate high resolution constraints on neu and neu\* transmembrane structures. These measurements can be made in membrane bilayer environments.

A.2 Polarized IR spectroscopy. The major objective of this section will be to map out other contact points along the dimer interface using cysteine sulphydryl exchange. The secondary structure and orientation of the neu and neu\* juxtamembrane sequences will also be established using attenuated total reflection FTIR spectroscopy. Local secondary structure will be characterized by site-directed isotope labeling and helix orientation will be characterized by amide I dichroism.

A.3 Molecular modeling. Based on the structural constraints obtained by polarized IR and MAS NMR methods, molecular dynamics and energy minimization protocols will be used to model the neu and neu\* transmembrane domains. The approach parallels that previously taken to obtain high resolution structural models of the transmembrane domains of glycophorin A and phospholamban (32,33).

## **B. Synthesis of competitive inhibitors of neu\*.**

### **B.1 Synthesis of neu transmembrane peptides with V664X substitutions.**

The first step towards designing competitive inhibitors to the neu and neu\* transmembrane domains is to measure the association energies of neu transmembrane peptides with several different amino acid substitutions at position 664. Peptides of different lengths will be synthesized incorporating all or part of the transmembrane sequence.

### **B.2 Dimerization assay of V664X transmembrane peptides.**

The association energies will be measured by fluorescence resonance energy transfer in a manner similar to that previously described for studying dimerization of the transmembrane domain of glycophorin A (13). Parameters that may influence dimerization (pH, temperature, lipid composition, ionic strength, etc.) will be systematically explored. Structural studies parallel to those outlined above will be undertaken on peptides exhibiting strong interactions.

### **B.3 Design of peptide mimetic inhibitors.**

Based on the results from A.1 and B.2, organic inhibitors (peptide and non-peptide) will be synthesized and compared. This technical objective heavily depends on the high resolution structural data and insights gained from the dimerization assays.

## **Technical Objectives 1-3: Structure of the neu and neu\* transmembrane and juxtamembrane domains. Years 1-2**

Task 1: Months 1-12: Polarized IR spectroscopy.

Task 2: Months 12-24: Magic angle spinning NMR spectroscopy.

Task 3: Months 1-48: Molecular modeling.

## **Technical Objectives 4-6: Synthesis of competitive inhibitors of neu\*. Years 2-4**

Task 4: Months 25-48: Synthesis of neu TM peptides with V664X substitutions.

Task 5: Months 25-48: Dimerization assay of V664X TM peptides.

Task 6: Months 36-48: Design of synthetic organic inhibitors.

### Task 1: Polarized IR Measurements on neu<sup>TM</sup> and neu<sup>\*</sup>TM.

Position 664 is the only established contact point in the neu<sup>\*</sup> dimer. The major thrust of this section of the proposal is to map out the interacting surfaces in the transmembrane dimer and determine whether or not there are multiple contact points. The approach we are using involves cysteine sulfhydryl exchange. The basis for the approach is that single cysteines provide unique markers for exchange. The SH groups in helix interfaces are protected from exchange in a manner analogous to the NH groups buried in the interior of soluble proteins. However, SH groups in the lipid interface undergo rapid SH to SD exchange from water which is known to readily permeate the lipid membrane. The SH vibrational mode is located at 2540 - 2590 cm<sup>-1</sup> away from other protein vibrations and shifts roughly -700 cm<sup>-1</sup> upon deuteration. The SH group is more acidic and more mobile than the backbone NH, and consequently exhibits faster exchange rates in membrane environments.

The first set of cysteine sulfhydryl exchange studies targeted the helical turns N-terminal to position 664. Cysteines have been incorporated into residues 656, 657, 658 and 661 in peptides with either valine or glutamate at position 664.

AEQRASP-C-TFIIATV-x-GVLLFLILVVVVGILIKRRRYK                      x = E OR V

AEQRASPV-C-FIIATV-x-GVLLFLILVVVVGILIKRRRYK

AEQRASPVT-C-IIATV-x-GVLLFLILVVVVGILIKRRRYK

AEQRASPVTFII-C-TV-x-GVLLFLILVVVVGILIKRRRYK

The sequences for the first four peptides that we targeted are given above. All experiments were carried out under reducing conditions. In each case studied, observation of an SH band at 2560 cm<sup>-1</sup> showed that the samples were reduced.

Figure 2 presents transmission FTIR spectra of the SD region of neu<sup>\*</sup>TM in DPPC membrane bilayers from two sites, position 657 and position 661. The results from the SH exchange studies are easy to interpret. If an SD band appears in D<sub>2</sub>O, then the site is not buried in a helix interface but exposed to lipid. The absence of an SD band in the A661C neu<sup>\*</sup>TM peptide indicates that position 661 is buried in the dimer interface. This results establishes a second contact point along the dimer interface in the activated neu<sup>\*</sup> receptor. The presence of an SD band in T657C (Figure 2, top) is consistent with this position being oriented towards the surrounding lipids. SD bands were also observed with the V656C and F658C neu<sup>\*</sup>TM peptides (data not shown). Measurements on both neu and neu<sup>\*</sup> sequences with cysteine substitutions on the C-terminal side of position 664 are currently in progress. These results are incorporated and discussed in the computational search and modeling section below (Task 3).

## Task 2: Magic Angle Spinning NMR Measurements of Intra- and Interhelical Contacts in neu\*TM.

The aim of the studies described in this section is to obtain distance constraints for the molecular modeling studies described under Task 3. We first describe measurements between  $^{13}\text{C}$  labels incorporated into the neu and neu\* transmembrane sequences in the vicinity of position 664. The spacing of the labels is sensitive to the transmembrane secondary structure.

Figure 3 presents the results of the intra-peptide RR NMR experiments. The experimental design of these experiments was described above in the *Procedures* section. The key data comes from the changes in intensity of the two  $^{13}\text{C}$  resonances. Large intensity changes correspond to short distances and small intensity changes correspond to long distances. The results are displayed as magnetization exchange curves which plot the normalized intensity differences between the two  $^{13}\text{C}$  resonances as a function of a mixing time. Figure 3a presents the magnetization exchange curves of  $[1\text{-}^{13}\text{C}\text{-Gly}^{665}, 3\text{-}^{13}\text{C}\text{-Ala}^{668}]$  neuTM and neu\*TM. In a canonical helix, these  $^{13}\text{C}$ -labels are separated by  $\sim 4.5$  Å. Simulations of the magnetization exchange are shown with solid lines for internuclear distances of 4.0, 4.5 and 5.0 Å using a zero quantum  $T_2$  of 1.6 ms.

Figure 3b presents the magnetization exchange curves of  $[1\text{-}^{13}\text{C}\text{-Thr}^{662}, 2\text{-}^{13}\text{C}\text{-Gly}^{665}]$  neuTM and neu\*TM. In a canonical helix, these  $^{13}\text{C}$ -labels are separated by  $\sim 4.8$  Å. Simulations of the magnetization exchange are shown with solid lines for internuclear distances of 4.0, 4.5 and 5.0 Å using a zero quantum  $T_2$  of 1.2 ms. The shorter zero quantum  $T_2$  value reflects the fact that the methylene  $\text{CH}_2$  group is harder to decouple than a methyl group. The zero quantum  $T_2$  parameter in general reflects intensity changes in the lines that are *not* due to the rotational resonance phenomenon. The values we have used were taken from independent spin echo linewidths. The fact that the simulations predict distances that are slightly shorter than those we expected for canonical helices is likely due to the fact that the zero quantum  $T_2$  parameter is underestimated. This places an error of  $\pm 0.3$  Å on all of the measurements in this study.

One of the goals of the proposed research is to test various models for the structure of neu\*TM and the structural changes occurring between neuTM and neu\*TM. The first model mentioned in the introduction involved a change in the secondary structure of the transmembrane domain between neuTM and neu\*TM. Brandt-Rauf et al. [5] calculated that the minimum-energy conformation of neuTM contains a sharp bend at positions 664 and 665, neu\*TM exists as an  $\alpha$ -helix. The intrahelical rotational resonance measurements discussed here have ruled out such a change in secondary structure.

Two additional models for receptor activation involve dimerization via hydrogen-bonding interactions [6]. In the first model, the helices are thought to be held in the "active" state by hydrogen bonding between the  $\text{Glu}^{664}$  COOH side chain on one helix and the  $\text{Glu}^{664}$  COOH side chain on the opposing helix. In the second model, the hydrogen bonding interactions are postulated to be between the  $\text{Glu}^{664}$  side chain and the peptide backbone carbonyl group of  $\text{Ala}^{661}$  of the second helix. The first set of interhelical measurements were aimed at the interaction between the  $\text{Glu}^{664}$  side chain and  $\text{Gly}^{665}$ .

Figure 4 presents the interhelical RR magnetization exchange curves for  $[5\text{-}^{13}\text{C-Glu}^{664}]$  neu\*TM reconstituted with  $[2\text{-}^{13}\text{C-Gly}^{665}]$  neu\*TM. The peptides were reconstituted in a 1:5 ratio and only the COOH intensity is plotted in Figure 4. This insures that ~85% of each  $[5\text{-}^{13}\text{C-Glu}^{664}]$  neu\* peptide interacts with a  $[2\text{-}^{13}\text{C-Gly}^{665}]$  neu\*TM peptide. Using the reconstitution protocol that involved detergent dialysis and sucrose gradients (but without incubation above the phase transition temperature), the data (solid circles) appear to be biphasic with a fast (~4 Å distance) and a slow component (> 5.5 Å distance). There are two possible explanations for this observation. First, the two glutamic acid groups in the dimer may have different conformations and correspondingly different distances to Gly<sup>665</sup>. The second possibility is that there are two (or more) dimer structures, one where the Glu - Gly distance is short and one where the distance is long. The idea in the second case is that one of the conformations is thermodynamically or kinetically trapped. To address this case, we incubated the sample above the phase transition temperature. Measurements after (open circles) incubation above the phase transition temperature of DMPC shows only the slow component. Simulations of the magnetization exchange are shown with solid lines for internuclear distances of 3.5, 4.0, 4.5 and 5.0 Å using a zero quantum  $T_2$  of 1.2 ms.

Based on the dimer structure of glycoporphin A where glycine residues are critical for dimerization (33), we targeted the distance between Gly residues across the dimer interface. Glycine has no side chain and potentially provides good van der Waals packing. Figure 5 presents interhelical RR magnetization exchange curves for  $[2\text{-}^{13}\text{C-Gly}^{665}]$  neu\*TM reconstituted with  $[1\text{-}^{13}\text{C-Gly}^{664}]$  neu\*TM (solid circles) and with wild-type  $[1\text{-}^{13}\text{C-Gly}^{664}]$  neuTM (open circles) in a 1:5 molar ratio. The neuTM - neu\*TM experiments were designed to test whether the mutant TM domain was also able to interact with the wild-type TM domain. Experiments were run after incubation for 12 h above the DMPC phase transition temperature. The Gly - Gly distance of 4 - 4.5 Å appears only slightly longer in the neu-neu\* heterodimer than in the neu\* homodimer. RR intensity changes of  $[2\text{-}^{13}\text{C-Gly}^{665}]$  neu\*TM reconstituted with  $[1\text{-}^{13}\text{C-Gly}^{664}]$  neu\*TM before incubation are shown in open squares. Simulations of the magnetization exchange are shown with solid lines for internuclear distances of 3.5, 4.0, 4.5 and 5.0 Å using a zero quantum  $T_2$  of 1.2 ms.

To further constrain the packing arrangement of the glycine residues in the interface, we also made RR measurements of  $[2\text{-}^{13}\text{C-Gly}^{665}]$  neu\*TM reconstituted with  $[1\text{-}^{13}\text{C-Ala}^{661}]$  neu\*TM in a 1:5 molar ratio. The data are plotted in Figure 6 and correspond to an internuclear distance of ~5 Å. The calculated distances in the structure proposed below are 4.1 and 7.4 Å.

Finally, the Gly-Gly experiments described above provide an indication as to the packing interface in neu\*, but do not address nature of the hydrogen-bonding partner or partners of Glu<sup>664</sup>. One possibility that emerged from the modeling studies below is that Glu<sup>664</sup> may be hydrogen-bonded to the polar threonine side chains at positions 657 and/or 662. Figure 7 presents RR magnetization exchange curves of  $[U\text{-}^{13}\text{C-Thr}^{662}, 5\text{-}^{13}\text{C-Glu}^{664}]$  neu\*TM reconstituted in DMPC. Simulations of the magnetization exchange are shown with solid lines for internuclear distances of 4.0, 4.5 and 5.0 Å using a zero quantum  $T_2$  of 1.6 ms. The measurements were made after incubation for 12 h and the estimated internuclear distance of 4.5 - 5 Å is shorter than the 5 - 6 Å internuclear distance between Glu<sup>664</sup> and Gly<sup>665</sup> shown in Figure 4 after incubation.

The distances between the  $^{13}\text{C}$ -labels discussed above are summarized in Table I in the appendix section.

### Task 3. Computational Searches for the neu\*TM Dimer Interface.

Recently, A. Brünger and coworkers have developed a computational search strategy for locating low energy conformations of dimers of transmembrane helices [32]. The approach has been used to locate the dimer interface between transmembrane helices of glycophorin A [33]. Low energy conformations of helix dimers are searched by rotating each helix through rotation angles  $\phi_1$  and  $\phi_2$  from 0 - 360° with a sampling size of 45°. The starting geometries include both left-handed and right-handed crossing angles.

Figure 8 presents the results of a computational search for the neu\*TM interface. This figure shows the cluster plot of low energy structures having left-handed crossing angles. Five left-handed clusters have been identified based on their final  $\phi_1$  and  $\phi_2$  angles, as well as their interaction energies and crossing angles. The initial grid, if shown, would display points separated by 45°. Figure 8 shows only those points that fall into a "cluster". These are the final minimized conformations that have migrated from their initial geometries and into low energy wells.

Figure 9 shows the low energy structures having right-handed crossing angles. Two right-handed clusters have been identified.

The orientations of Glu<sup>664</sup> (red) and Gly<sup>665</sup> (yellow) for each of the seven clusters (both left and right-handed structures) are shown in Figure 10 (viewed down the helix axis of the one of the monomers in the dimer). Both Glu<sup>664</sup> and Gly<sup>665</sup> might be expected to be in the interface based on the mutagenesis studies of Stern and coworkers [4]. Two clusters (cluster 4 and 7) are roughly symmetric. The interaction energy of cluster 7 at -126.2 kcal/mole is much lower than that of cluster 4. In these simulations the dielectric constant is assumed to be  $\epsilon=2$  and the interaction energy is driven by helix-helix interactions (both favorable and unfavorable).

Three parameters make up the input for any given computational search: the peptide sequence, the sampling step size and the helix-helix separation. The initial searches start with a step size of 45°, but this is narrowed once candidate clusters have been identified. The helix-helix separation can range from ~10.0 - 11.5 Å. The calculations shown in Figures 8-10 are based on a helix-helix separation of 10.5 Å. Helix-helix separations of 11.0 and 11.5 Å gave similar results, however with a separation of 10.0 Å the Glu<sup>664</sup> side chains did not interact with the opposing helix.

Figure 11 presents the low energy structures of neuTM and neu\*TM homodimers. (For neu\*TM, this is cluster 7 in Figures 9 and 10). In both cases the low energy structure predicts that Gly<sup>665</sup> packs in the dimer interface. In neuTM (with valine at position 664), this is a left-handed coiled coil, while for neu\*TM a right-handed geometry is predicted. The most stabilizing interactions in neu\*TM come from interhelical hydrogen-bonding of the Glu<sup>664</sup> carboxyl side side with the hydroxyl side chains of Thr<sup>657</sup> and Thr<sup>662</sup>. The structure is not completely symmetric. Hydrogen-bonding of Glu<sup>664</sup> with Thr<sup>662</sup> is supported by the rotational resonance NMR measurements in Figure 7. The neu\*TM structure in Figure 11 is also consistent with the SH exchange data which show that position 661 is buried in the dimer interface and unable to exchange.

Figure 12 again presents the low energy structure of neu\*TM homodimer. The inset shows the neu\*TM dimer with a 40° crossing angle in agreement with our polarized IR measurements. The relatively large crossing angle is thought to facilitate orientation of the intracellular kinase domains. At



this stage the distances obtained in the NMR experiments have not been used as restraints or constraints to guide the final modeling. This will be done in the coming year. The comparison of the distances obtained by experiment and by computational searching show that we are not far off. This parallel approach bolsters our confidence in the results of both the NMR measurements and the computational searches.

## CONCLUSIONS

The objective of the current DAMD grant is to establish high resolution structural constraints on the transmembrane domain of the neu/erbB-2 receptor in membrane environments. Such data addresses specific models for receptor activation by the transforming Glu<sup>664</sup> mutation. The ultimate goal is to obtain high resolution 3D structures of the neuTM and neu\*TM domains that can be used to establish the activation mechanism and that serve as guides to the design of competitive inhibitors. The results presented above demonstrate we are well on the way to completing these aims. The conclusions that can be drawn thus far are as follows:

- Glu<sup>664</sup> drives the dimerization of the neu\* transmembrane domain through hydrogen-bonding interactions.
- Gly<sup>665</sup> and Ala<sup>661</sup> pack in the dimer interface and stabilize the helix dimer through van der Waals interactions.
- The polar threonine residues at positions 662 and 657 are likely to be involved in stabilizing the active neu\* dimer through hydrogen bonding interactions.
- Computational searches predict a left-handed geometry for the neu transmembrane sequence and a right-handed geometry for neu\* transmembrane sequence.
- The secondary structure of the neu and neu\* transmembrane sequences is the same. The activating mutation does not induce a large change in secondary structure.

In terms of designing competitive inhibitors, two major conclusions can be drawn from these studies thus far.

- Specific inhibitors to the neu\* sequence should target the polar threonine and glutamic acid residues as well as the van der Waals surfaces created by Gly<sup>665</sup> and Ala<sup>661</sup>, both of which have small side chains and allow good packing interactions.
- Specific inhibitors to the neu sequence should target the polar threonine residues as well as Gly<sup>665</sup> and Ala<sup>661</sup>. Inhibitors to the neu sequence are of importance because overexpression of the wild-type receptor leads to receptor activation. The observation that Gly<sup>665</sup> is likely in the dimer interface of both neu and neu\* is consistent with a common orientation and mechanism of activation.

## REFERENCES

- 1 Bargmann CI, Weinberg RA. Oncogenic activation of the neu-encoded receptor protein by point mutation and deletion. *EMBO J* 1988; 7:2043-2052.
- 2 Bargmann CI, Hung M-C, Weinberg RA. Multiple independent activations of the neu oncogene by a point mutation altering the transmembrane domain of p185. *Cell* 1986; 45:649-657.
- 3 Bargmann CI, Hung M-C, Weinberg RA. The neu oncogene encodes an epidermal growth factor receptor-related protein. *Nature* 1986; 319:226-230.
- 4 Cao H, Bangalore L, Bormann B-J, Stern DF. A subdomain in the transmembrane domain is necessary for p185neu\* activation. *EMBO J* 1992; 11:923-932.
- 5 Brandt-Rauf PW, Rackovsky S, Pincus MR. Correlation of the structure of the transmembrane domain of the neu oncogene-encoded p185 protein with its function. *Proc Natl Acad Sci U S A* 1990; 87:8660-8664.
- 6 Sternberg MJ, Gullick WJ. Neu receptor dimerization. *Nature* 1989; 339:587.
- 7 Weiner DB, Liu J, Cohen FA, Williams WV, Greene MI. *Nature* 1989; 339:230-231.
- 8 Lofts FJ, Hurst HC, Sternberg MJE, Gullick WJ. Specific short transmembrane sequences can inhibit transformation by the mutant neu growth factor receptor in vitro and in vivo. *Oncogene* 1993; 8:2813-2820.
- 9 Arkin IT, Rothman M, Ludlam CFC, Aimoto S, Engelman DE, Rothschild K, Smith SO. Structural model of the phospholamban ion channel complex in phospholipid membranes. *J Mol Biol* 1995; 248:824-834.
- 10 Smith SO, Jonas R, Braiman M, Bormann BJ. Structure and orientation of the transmembrane domain of glycophorin A in lipid bilayers. *Biochemistry* 1994; 33:6334-6341.
- 11 Smith SO, Bormann BJ. Determination of helix-helix interactions in membranes by rotational resonance NMR. *Proc Natl Acad Sci USA* 1995; 92:488-491.
- 12 Levitt MH, Raleigh DP, Creuzet F, Griffin RG. Theory and simulations of homonuclear spin pair systems in rotating solids. *J Chem Phys* 1990; 92:6347.
- 13 Gullion T, Schaefer J. Detection of weak heteronuclear dipolar coupling by rotational echo double-resonance nuclear magnetic resonance. *Adv Magn Reson* 1989; 13:57-83.
- 14 Hing AW, Vega S, Schaefer J. Transferred-echo double resonance NMR. *J Magn Reson* 1992; 96:205-209.
- 15 Tycko R, Smith SO. Symmetry principles in the design of pulse sequences for structural measurements in magic angle spinning nuclear magnetic resonance. *J Chem Phys* 1993; 98:932-943.

- 16 Colombo MG, Meier BH, Ernst RR. Rotor-driven spin diffusion in natural-abundance  $^{13}\text{C}$  Spin Systems. *Chem Phys Lett* 1988; 146:189-196.
- 17 Peersen OB, Yoshimura S, Hojo H, Aimoto S, Smith SO. Short range distance determination in integral membrane proteins by magic angle spinning NMR. *J Am Chem Soc* 1992; 114:4332-4335.
- 18 Peersen OB, Groesbeek, M, Aimoto, S., Smith SO. Analysis of rotational resonance magnetization exchange curves from crystalline peptides 1995; 117:7228-7237.
- 19 Bork V, Gullion T, Hing A, Schaefer J. Measurement of  $^{13}\text{C}$  -  $^{15}\text{N}$  coupling by dipolar-rotational spin-echo NMR. *J Magn Reson* 1990; 88:523-532.
- 20 Gullion T, Schaefer J. Rotational-Echo Double-Resonance NMR. *J Magn Reson* 1988; 81:196-200.
- 21 Braiman MS, Rothschild KJ. Fourier transform infrared techniques for probing membrane protein structure. *Ann Rev Biophys Biophys Chem* 1989; 17:541-570.
- 22 Kauppinen JK, Moffatt DJ, Mantsch HH, Cameron DG. Fourier self-deconvolution: A method for resolving intrinsically overlapped bands. *Appl Spectrosc* 1981; 35:271-276.
- 23 Byler MD, Susi H. Examination of the secondary structure of proteins by Deconvolved FTIR spectra. *Biopolymers* 1986; 25:469-487.
- 24 Bradbury EM, Brown L, Downie AR, Elliott A, Fraser RDB, Hanby WE. The structure of the  $\omega$ -form of poly- $\beta$ -benzyl-L-aspartate. *J Mol Biol* 1962; 5:230-247.
- 25 Miyazawa T, Blout ER. The infrared spectra of polypeptides in various conformations: amide I and amide II bands. *J Am Chem Soc* 1961; 83:712-719.
- 26 Tsuboi M. Infrared dichroism and molecular conformation of  $\alpha$ -form poly- $\gamma$ -benzyl-L-glutamate. *J Polymer Sci* 1994; 59:139-153.
- 27 Gu Z, Zambrano R, McDermott A. Hydrogen bonding of carboxyl groups in solid-state amino acids and peptides: comparison of carbon chemical shielding, infrared frequencies, and structures. *J Am Chem Soc* 1994; 116:6368-6372.
- 28 Hamilton JA, Cistola DP. Transfer of oleic acid between albumin and phospholipid vesicles. *Proc Natl Acad Sci USA* 1986; 83:82-86.
- 29 Kantor HL, Prestegard JP. Fusion of phosphatidylcholine bilayer vesicles: role of free fatty acid. *Biochemistry* 1978; 17:3592-3597.
- 30 Ptak M, Egret-Charlier M, Sanson A, Bouloussa O. A NMR study of the ionization of fatty acids, fatty amines and N-acylamino acids incorporated in phosphatidylcholine vesicles. *Biochim Biophys Acta* 600:387-397 (1980).

- 31 Arkin, I.T., Mackenzie, K., Aimoto, S., Engelman, D. and S.O. Smith Mapping the lipid exposed surface of membrane proteins. *Nature Struct. Biol.* 3, 240-243 (1996).
- 32 Adams, PD, Arkin, IT, Engelman, DM, Brunger, AT. Computational searching and mutagenesis suggest a structure for the pentameric transmembrane domain of phospholamban. *Nature Struct. Biol.* 2, 154-162 (1995).
33. Treutlein, HR, Lemmon, M, Engelman, DM, Brunger, AT. The glycophorin A transmembrane domain dimer: sequence specific propensity for a right-handed supercoil of helices. *Biochemistry* 31, 12726-12733 (1992).

## Appendices

Table 1

<u>Sample</u>	<u>Experimental Distance</u>	<u>Calculated Distance</u>
[1- <sup>13</sup> C-Gly <sup>665</sup> , 3- <sup>13</sup> C-Ala <sup>668</sup> ] neu*TM	4.3-4.4 Å	4.5 Å
[1- <sup>13</sup> C-Gly <sup>665</sup> , 3- <sup>13</sup> C-Ala <sup>668</sup> ] neuTM	4.3-4.4 Å	4.5 Å
[1- <sup>13</sup> C-Thr <sup>662</sup> , 2- <sup>13</sup> C-Gly <sup>665</sup> ] neu*TM	4.5-4.7 Å	4.8 Å
[1- <sup>13</sup> C-Thr <sup>662</sup> , 2- <sup>13</sup> C-Gly <sup>665</sup> ] neuTM	4.5-4.7 Å	4.8 Å
[5- <sup>13</sup> C-Glu <sup>664</sup> ] neu*TM <-> [2- <sup>13</sup> C-Gly <sup>665</sup> ] neu*TM	> 5.0 Å	5.8 and 6.5 Å
[2- <sup>13</sup> C-Gly <sup>665</sup> ] neu*TM <-> [1- <sup>13</sup> C-Gly <sup>664</sup> ] neu*TM	4.0 Å	4.1 Å
2- <sup>13</sup> C-Gly <sup>665</sup> ] neu*TM <-> [1- <sup>13</sup> C-Gly <sup>664</sup> ] neuTM	4.4 Å	4.2 Å
[2- <sup>13</sup> C-Gly <sup>665</sup> ] neu*TM <-> [1- <sup>13</sup> C-Ala <sup>661</sup> ] neu*TM	4.5 - 5.0 Å	4.1 and 7.4 Å
[CH <sub>3</sub> - <sup>13</sup> C-Thr <sup>662</sup> , 5- <sup>13</sup> C-Glu <sup>664</sup> ] neu*TM	4.2 - 5.0 Å	4.4 and 6.3 Å

## Figure Legends

Figure 1: Helical wheel diagram of the erbB-2 transmembrane domain. Residues from Leu<sup>670</sup> to Ala<sup>653</sup> are shown in a canonical  $\alpha$ -helix having 3.6 residues per turn.

Figure 2: Polarized transmission FTIR spectra of the SD region of neu\*TM in DPPC membrane bilayers. Cysteine substitutions were made at Thr 657 (a) and at Ala 661 (b). The absence of an SD band in the A661C neu\*TM peptide suggests that position 661 is buried in the dimer interface. The sample chamber was purged with nitrogen, and the samples layered on a Ge crystal plate and dried using argon or nitrogen. Each spectrum represents the average of 1000 scans acquired at a resolution of 4 cm<sup>-1</sup>.

Figure 3: Intrahelical <sup>13</sup>C RR magnetization exchange curves. (a) Intensity differences of [<sup>1-13</sup>C-Gly<sup>665</sup>, <sup>3-13</sup>C-Ala<sup>668</sup>] neuTM and neu\*TM peptides as a function of mixing time. In a canonical helix, these <sup>13</sup>C-labels are separated by ~4.5 Å. Simulations of the magnetization exchange are shown with solid lines for internuclear distances of 4.0, 4.5 and 5.0 Å using a zero quantum T<sub>2</sub> of 1.6 ms. (b) Intensity differences of [<sup>1-13</sup>C-Thr<sup>662</sup>, <sup>2-13</sup>C-Gly<sup>665</sup>] neuTM and neu\*TM peptides as a function of mixing time. In a canonical helix, these <sup>13</sup>C-labels are separated by ~4.8 Å. Simulations of the magnetization exchange are shown with solid lines for internuclear distances of 3.5, 4.0, 4.5 and 5.0 Å using a zero quantum T<sub>2</sub> of 1.2 ms.

Figure 4: Interhelical RR magnetization exchange curves for neu\*TM. RR intensity changes of [<sup>5-13</sup>C-Glu<sup>664</sup>] neu\*TM reconstituted with [<sup>2-13</sup>C-Gly<sup>665</sup>] neu\*TM. Measurements were made before (solid circles) and after (open circles) incubation above the phase transition temperature of DMPC. Before incubation the curves appear to be biphasic with a fast (~4 Å distance) and a slow component (> 5.5 Å distance). The fast component disappears upon incubation. Simulations of the magnetization exchange are shown with solid lines for internuclear distances of 3.5, 4.0, 4.5 and 5.0 Å using a T<sub>2</sub> of 1.2 ms.

Figure 5: Interhelical RR magnetization exchange curves for neu\*TM-neu\*TM and neu\*TM-neuTM dimers. RR intensity changes of [<sup>2-13</sup>C-Gly<sup>665</sup>] neu\*TM reconstituted with [<sup>1-13</sup>C-Gly<sup>665</sup>] neu\*TM (solid circles) and with wild-type [<sup>1-13</sup>C-Gly<sup>665</sup>] neuTM (open circles) in a 1:5 molar ratio. Experiments were run after incubation for 12 h above the DMPC phase transition temperature. The Gly - Gly distance of 4 - 4.5 Å appears only slightly longer in the neu-neu\* heterodimer than in the neu\* homodimer. RR intensity changes of [<sup>2-13</sup>C-Gly<sup>665</sup>] neu\*TM reconstituted with [<sup>1-13</sup>C-Gly<sup>665</sup>] neu\*TM before incubation are shown in open squares. Simulations of the magnetization exchange are shown with solid lines for internuclear distances of 3.5, 4.0, 4.5 and 5.0 Å using a zero quantum T<sub>2</sub> of 1.2 ms.

Figure 6: Interhelical rotational resonance NMR magnetization exchange curves for neu\*TM. (a) RR intensity changes of [<sup>2-13</sup>C-Gly<sup>665</sup>] neu\*TM reconstituted with [<sup>1-13</sup>C-Gly<sup>665</sup>] neu\*TM in a 1:5 molar ratio. The internuclear distance is estimated to be ~4 Å close to the 4.06 Å distance in the calculated structure. (b) RR intensity changes of [<sup>2-13</sup>C-Gly<sup>665</sup>] neu\*TM reconstituted with [<sup>1-13</sup>C-Ala<sup>661</sup>] neu\*TM in a 1:5 molar ratio. The internuclear distance is estimated to be ~5 Å. The calculated distances in the structure proposed below are 4.1 and 7.4 Å. Simulations are shown in both curves for internuclear distances of 3.5, 4.0, 4.5 and 5.0 Å using a zero quantum T<sub>2</sub> of 1.2 ms.

Figure 7: RR intensity changes of [U- $^{13}\text{C}$ -Thr $^{662}$ , 5- $^{13}\text{C}$ -Glu $^{664}$ ] neu\*TM reconstituted in DMPC. Simulations of the magnetization exchange are shown with solid lines for internuclear distances of 4.0, 4.5 and 5.0 Å using a zero quantum  $T_2$  of 1.6 ms. The measurements were made after incubation for 12 h and the estimated internuclear distance of 4.5 - 5 Å is shorter than the 5 - 6 Å internuclear distance between Glu $^{664}$  and Gly $^{665}$  shown in Figure 4 after incubation.

Figure 8: Computational search for neu\*TM interface. Cluster plot showing low energy structures having left-handed crossing angles.

Figure 9: Computational search for neu\*TM interface. Cluster plot showing low energy structures having right-handed crossing angles.

Figure 10: Structures from computational search of neu\*TM dimers. Seven clusters were identified. Two clusters (cluster 4 and 7) are roughly symmetric. Interaction energies are listed.

Figure 11: Low energy structures of neuTM and neu\*TM homodimers. In both cases the low energy structure predicts that the Gly $^{665}$  packs in the dimer interface.

Figure 12: Low energy structure of the neu\*TM homodimer. The inset shows the neu\*TM dimer with a 40° crossing angle in agreement with polarized IR measurements.



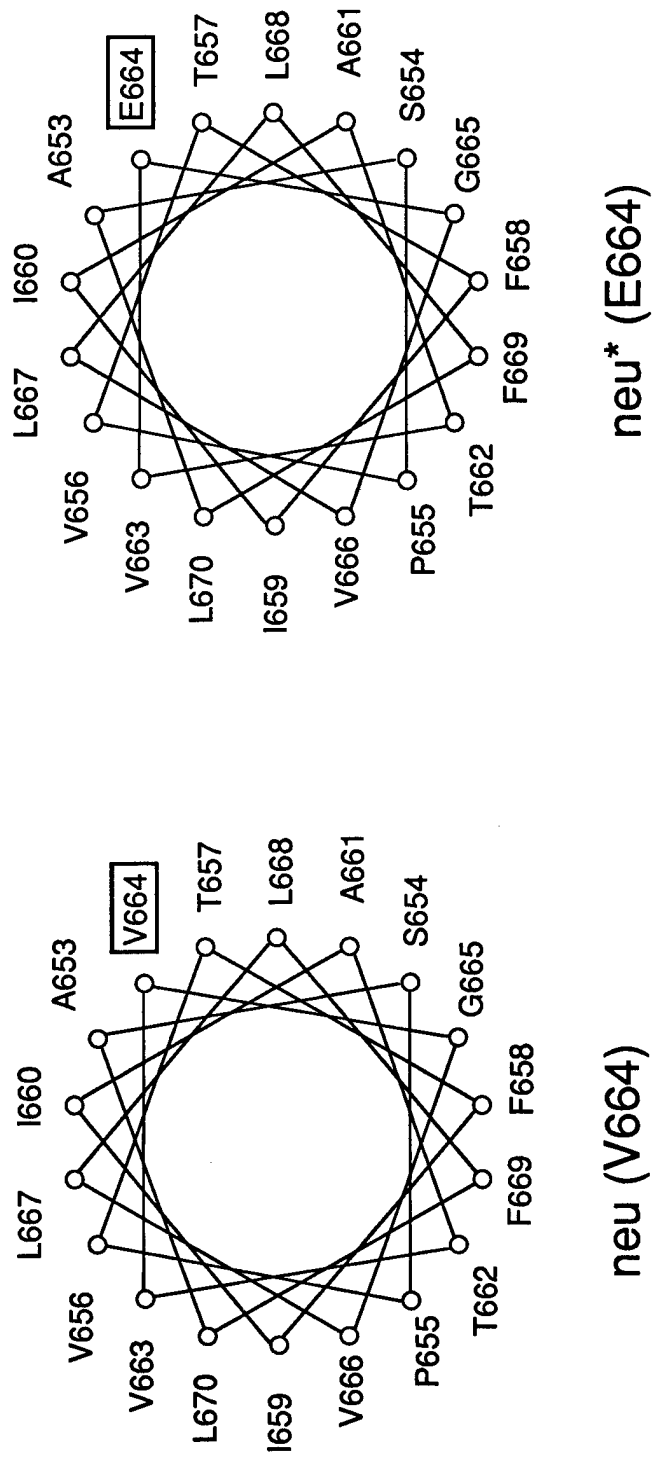


FIGURE 1

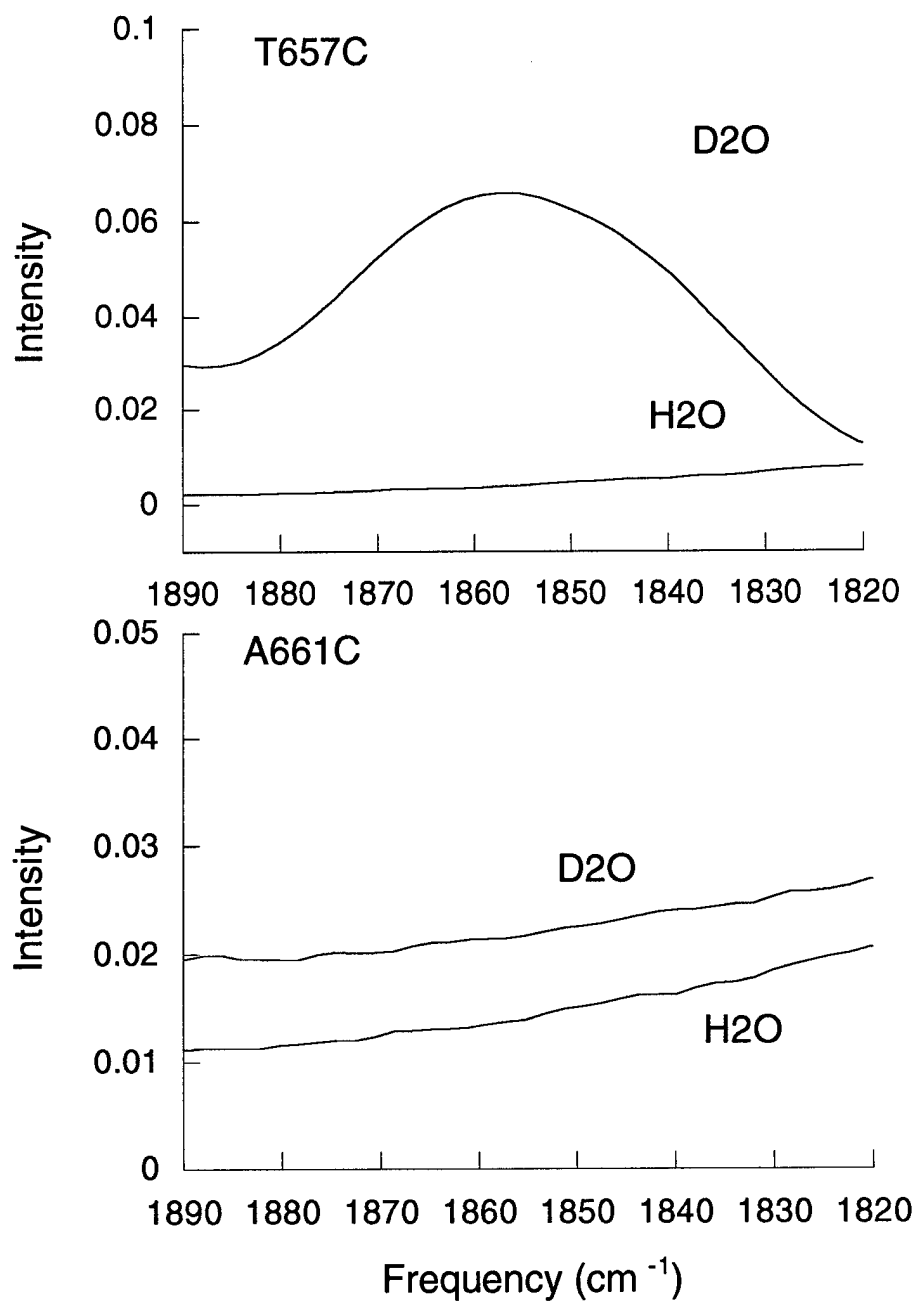


FIGURE 2

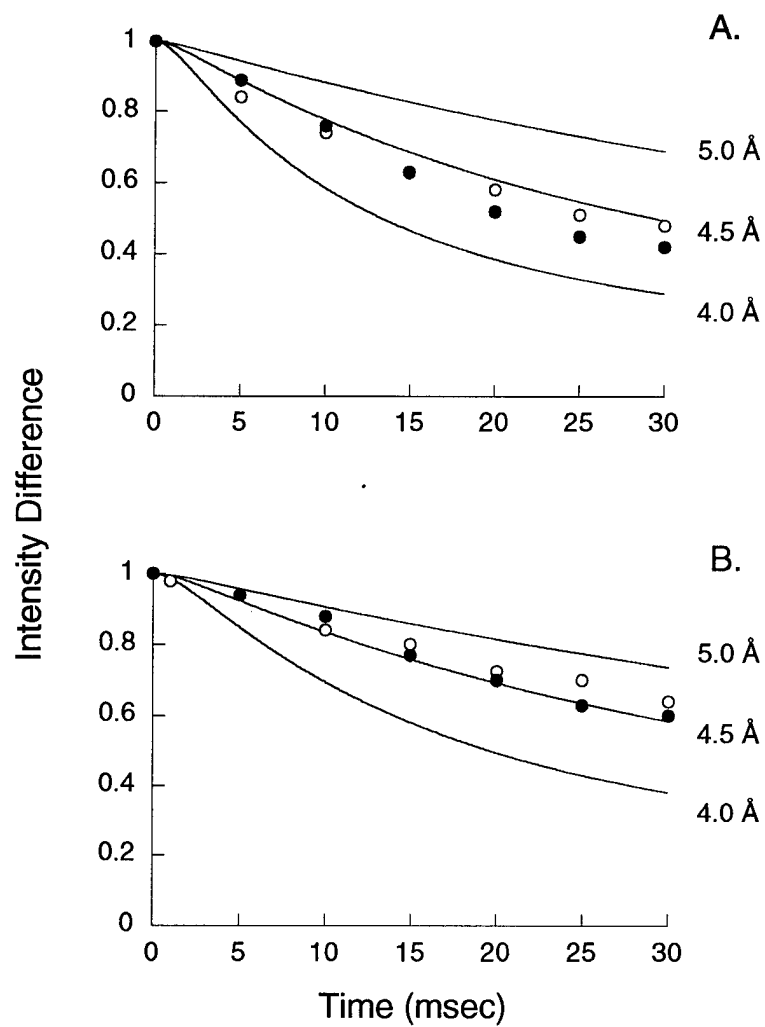


FIGURE 3

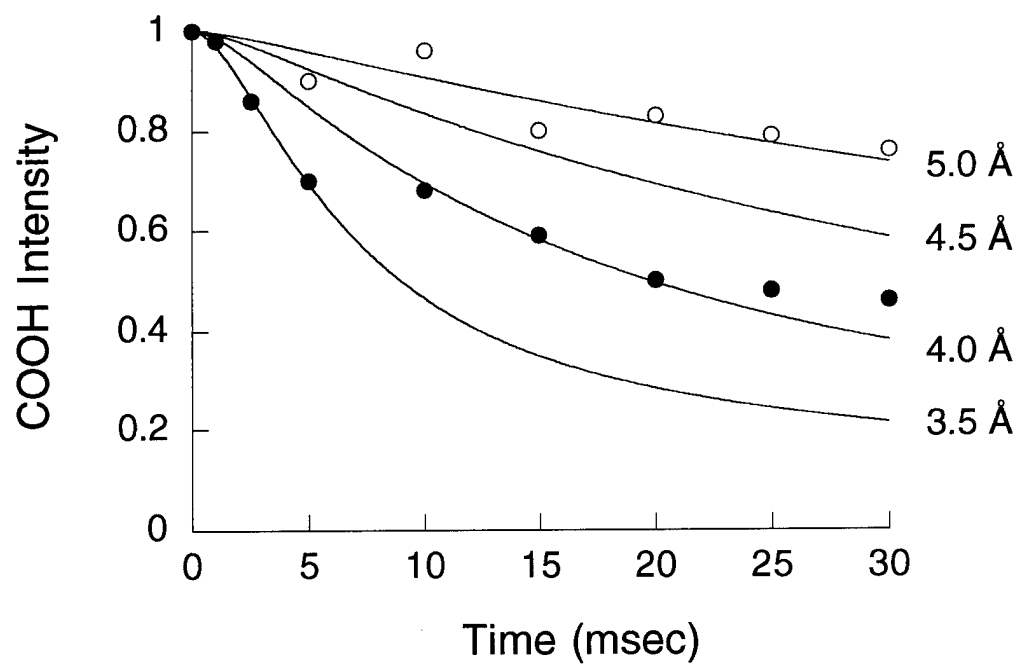


FIGURE 4

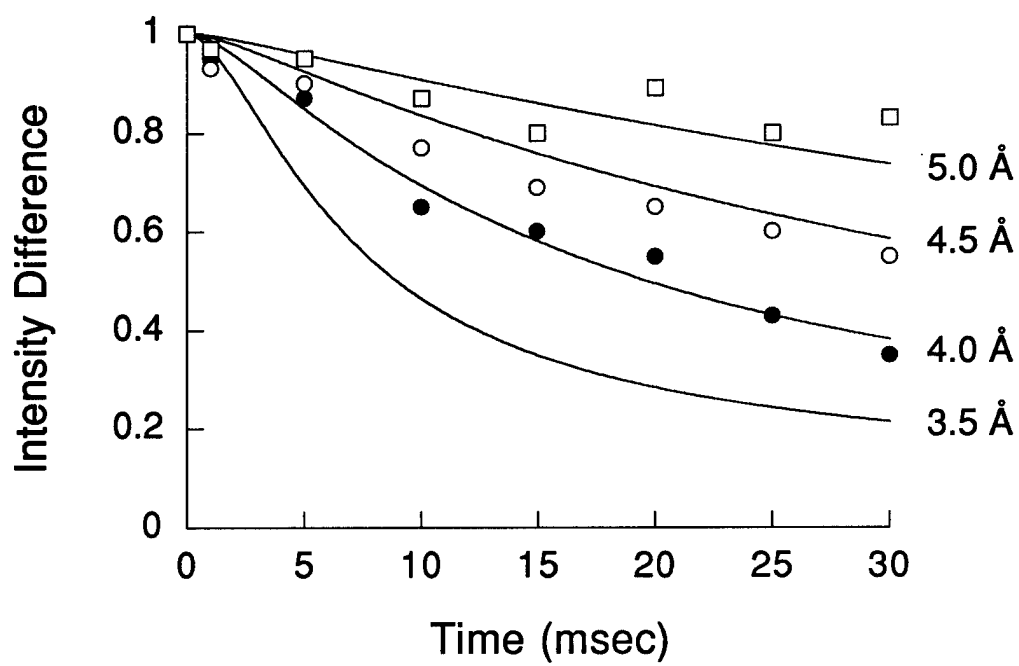


FIGURE 5

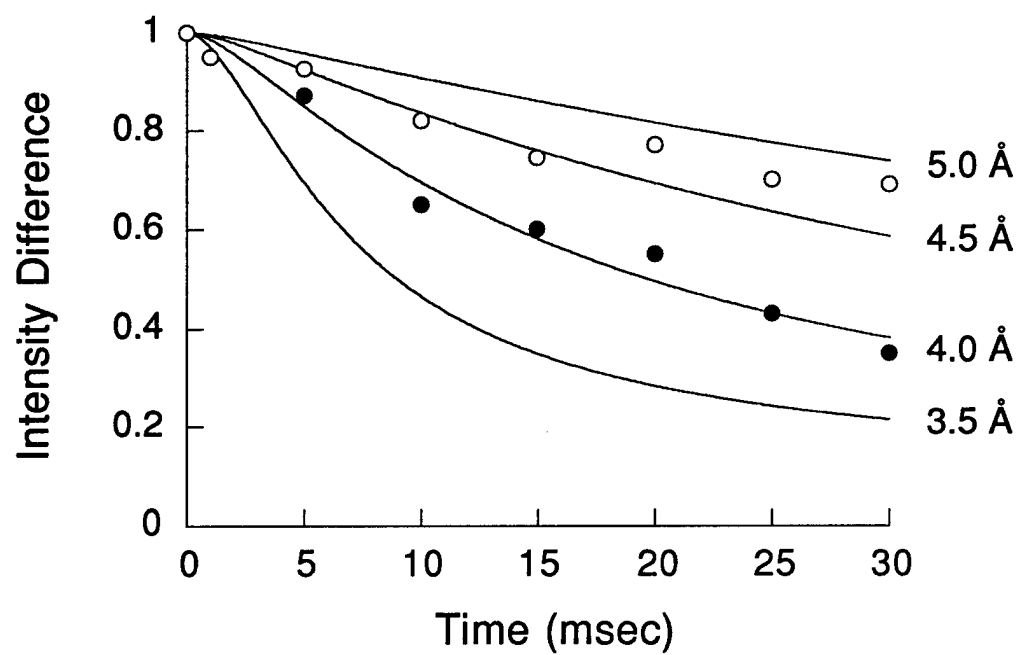


FIGURE 6

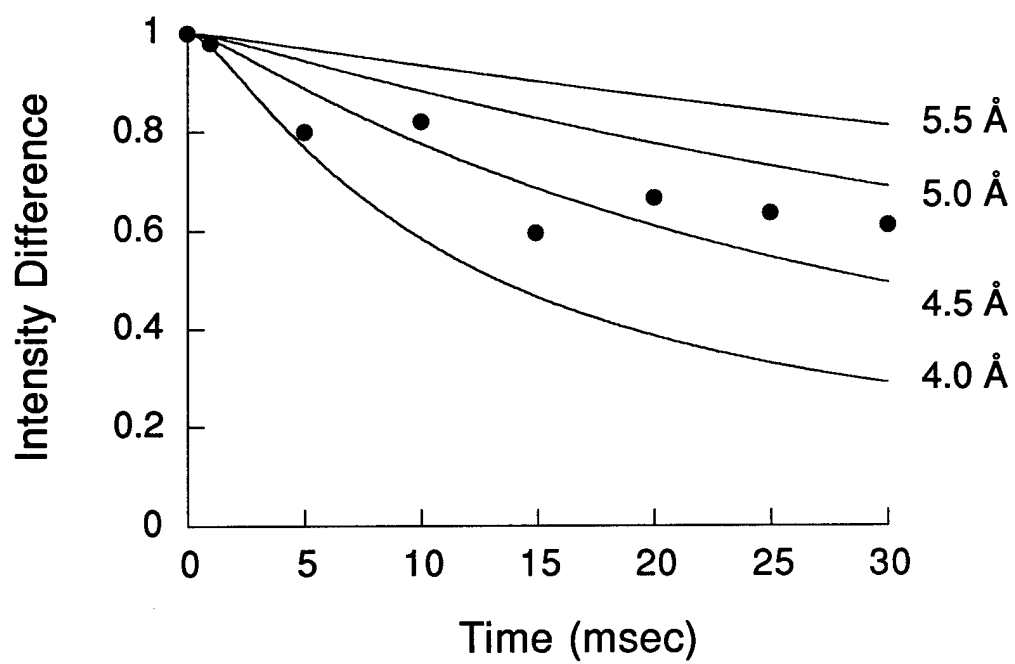


FIGURE 7

neu\_wt left handed structures

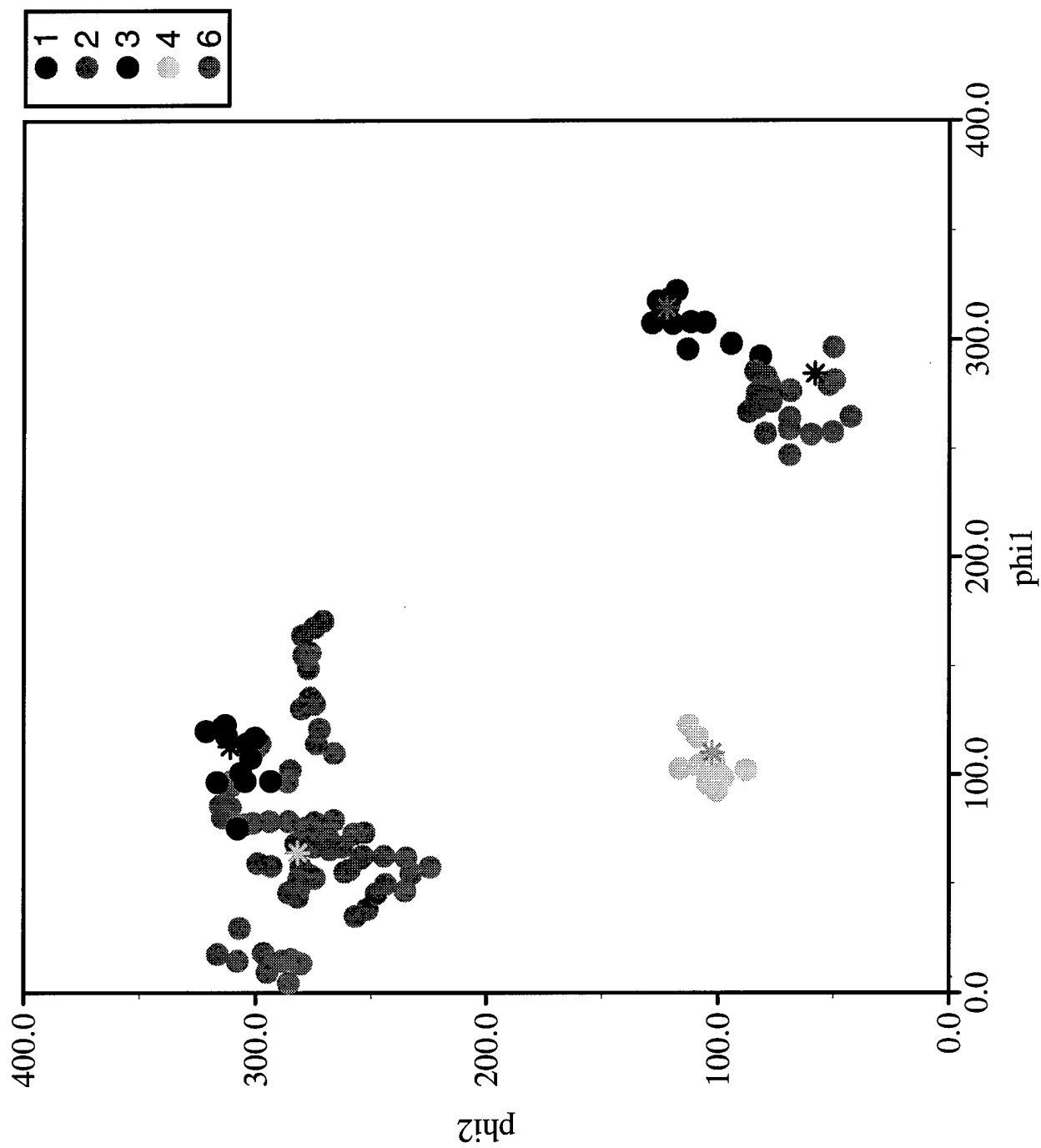


FIGURE 8



neu\_wt right handed structures

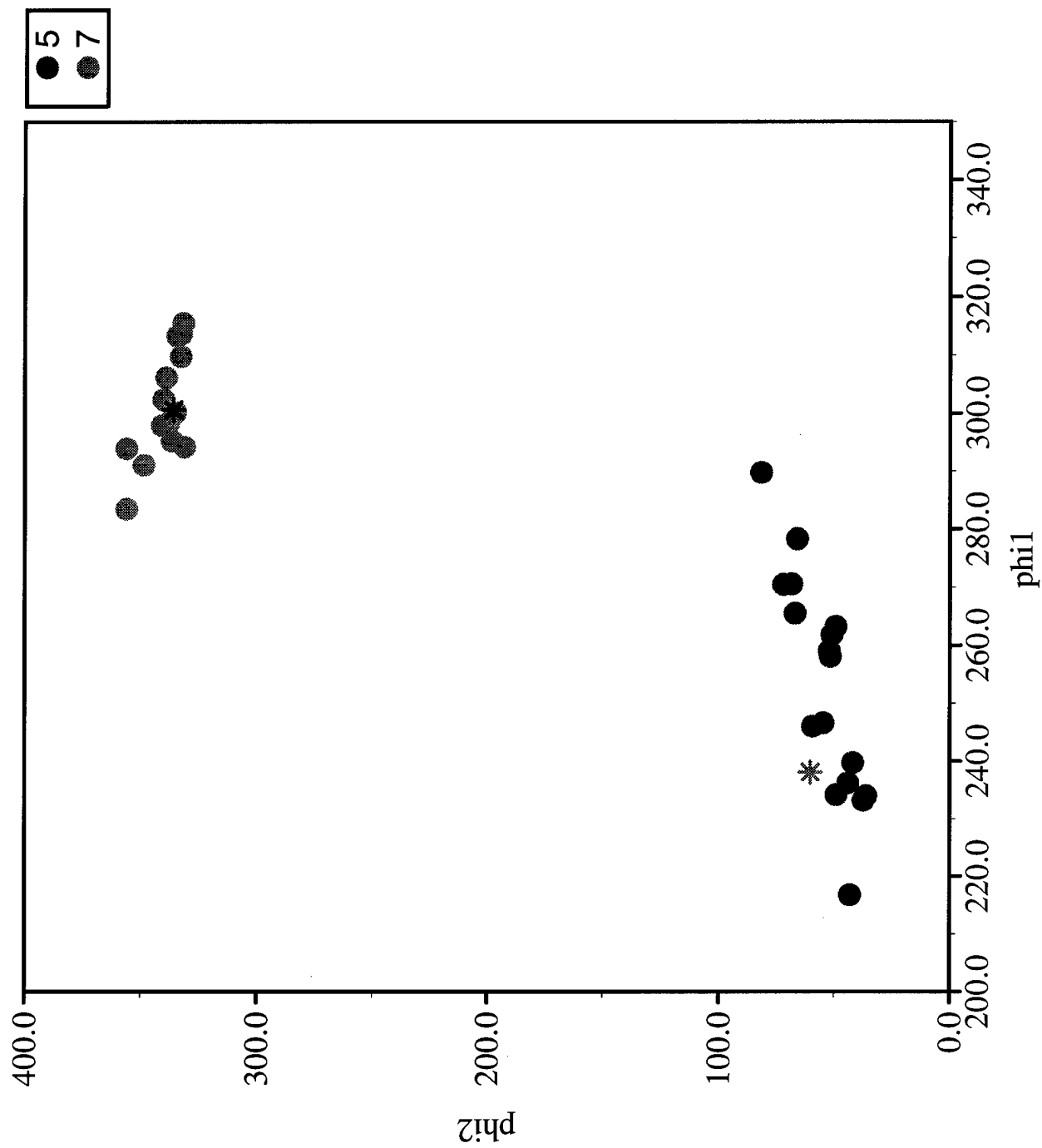


FIGURE 9

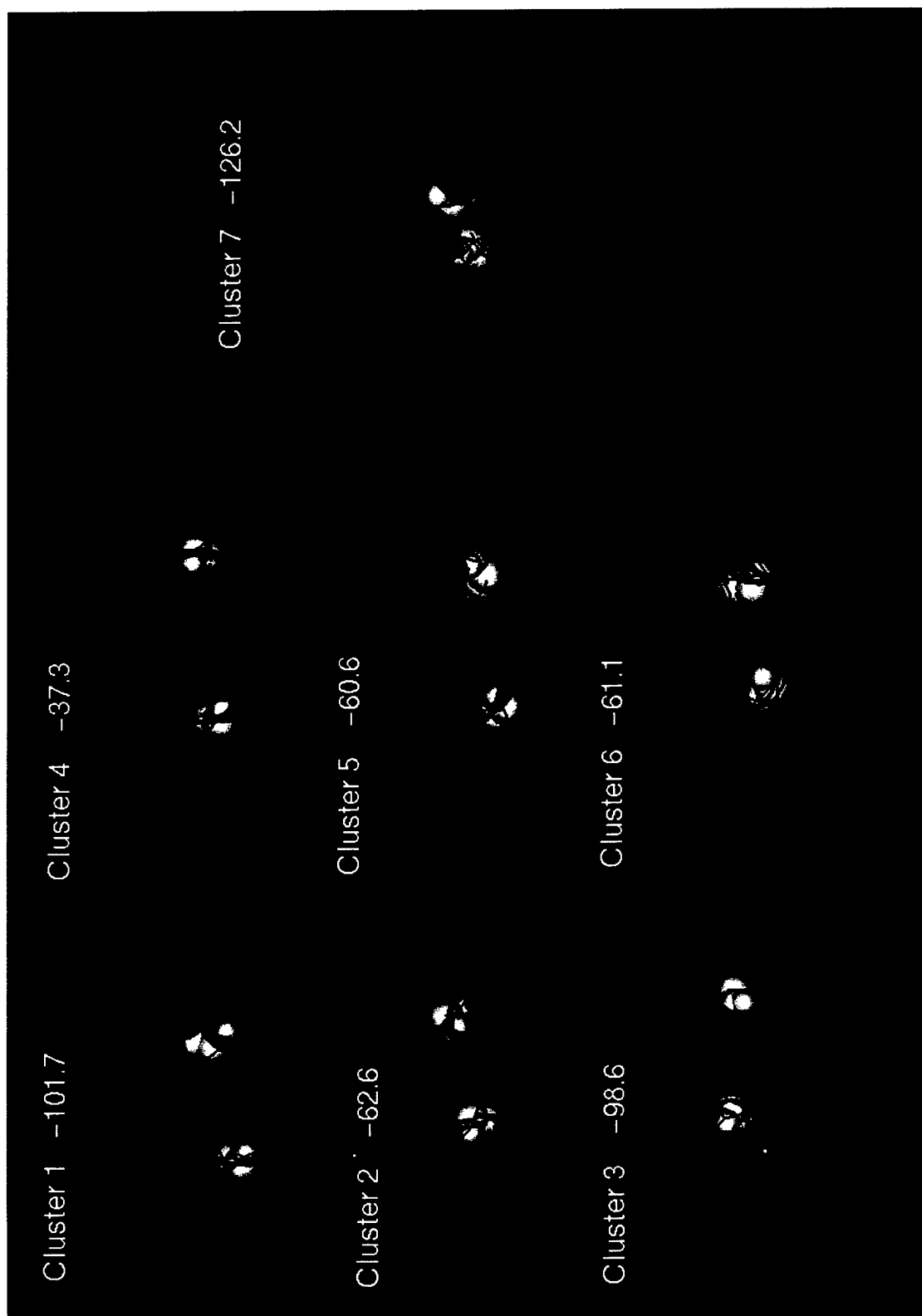


FIGURE 10

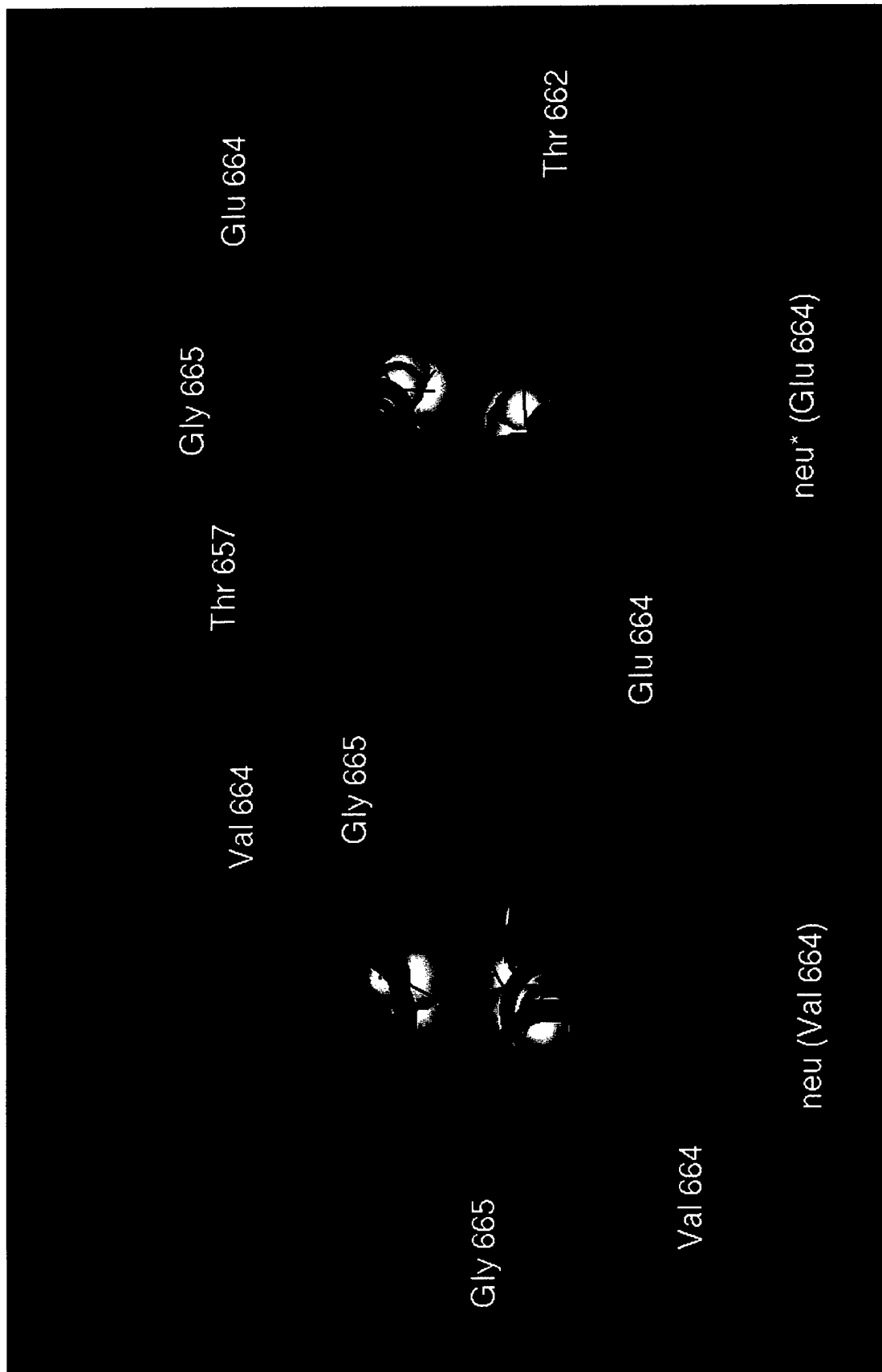


FIGURE 11

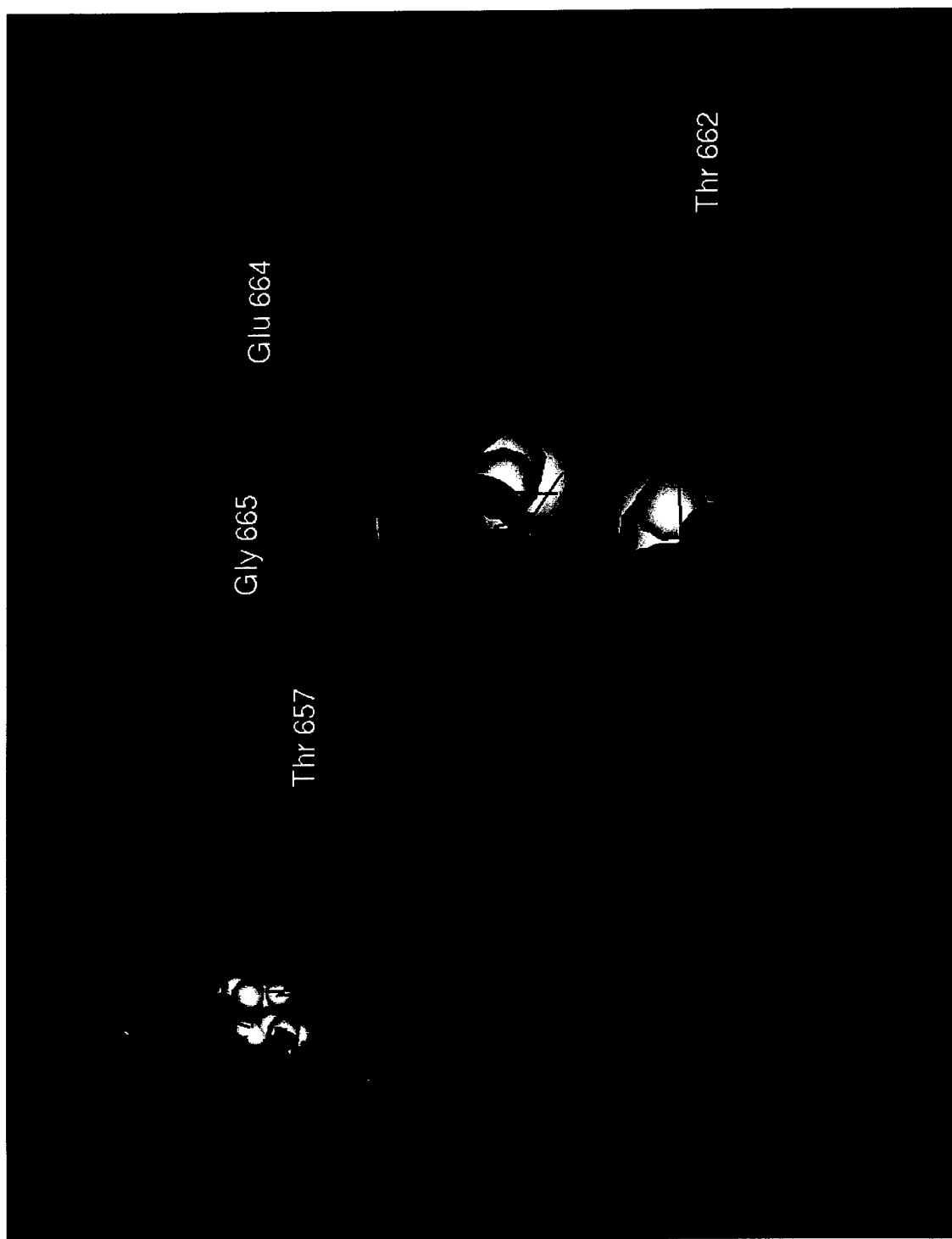


FIGURE 12